Scatter correction method for cone-beam CT based on interlacing-slit scan*

Huang Kui-Dong(黄魁东)[a)†], Zhang Hua(张 华)[b)], Shi Yi-Kai(史仪凯)[b)], Zhang Liang(张 亮)[a)], and Xu Zhe(徐 哲)[a)]

[a)] *Key Laboratory of Contemporary Design and Integrated Manufacturing Technology of the Ministry of Education, Northwestern Polytechnical University, Xi'an* 710072, *China*

[b)] *School of Mechanical Engineering, Northwestern Polytechnical University, Xi'an* 710072, *China*

(Received 4 November 2013; revised manuscript received 3 March 2014; published online 16 July 2014)

Cone-beam computed tomography (CBCT) has the notable features of high efficiency and high precision, and is widely used in areas such as medical imaging and industrial non-destructive testing. However, the presence of the ray scatter reduces the quality of CT images. By referencing the slit collimation approach, a scatter correction method for CBCT based on the interlacing-slit scan is proposed. Firstly, according to the characteristics of CBCT imaging, a scatter suppression plate with interlacing slits is designed and fabricated. Then the imaging of the scatter suppression plate is analyzed, and a scatter correction calculation method for CBCT based on the image fusion is proposed, which can splice out a complete set of scatter suppression projection images according to the interlacing-slit projection images of the left and the right imaging regions in the scatter suppression plate, and simultaneously complete the scatter correction within the flat panel detector (FPD). Finally, the overall process of scatter suppression and correction is provided. The experimental results show that this method can significantly improve the clarity of the slice images and achieve a good scatter correction.

Keywords: cone-beam computed tomography, scatter correction, interlacing slits, image fusion

PACS: 81.70.Tx, 87.57.Q–, 87.64.Bx, 87.57.C– **DOI:** 10.1088/1674-1056/23/9/098106

1. Introduction

In a cone-beam computed tomography (CBCT) system, the projection images of a tested object are collected from a flat panel detector (FPD) when the cone beam X-ray source is on, then serial slice images are reconstructed with the corresponding reconstruction algorithm from these images. The CBCT has many advantages, such as high scan speed, the same space distinguishing ratio in the slice inner and between slices, and high precision. The CBCT has been extensively applied in medical imaging and industrial non-destructive testing.[1,2]

The scatter is an important factor which can influence the image quality in the CT imaging process. Due to the existence of the scatter, the image contrast is reduced,[3] and the image details become blurred. It is very negative for the detection of tiny structures or defects. The scatter intensity and distribution are not only related with the ray energy, but also related with the material, structure, thickness, area, and even the whole imaging environment. As there are so many uncertain factors, the scatter correction is still a focused problem to be solved.[4–7]

The scatter suppression and correction techniques can be generally divided into two types: hardware methods and software methods.[8] The hardware methods, which consider the geometry conditions of the X-ray imaging, can reduce the amount of scatter reaching the detector by means of adding hardware devices. The hardware methods mainly include collimator, air gap,[9] bucky,[10] radiopaque strips, honeycomb grid,[11] and so on. The software methods, which handle the projection images based on digital image processing methods, obtain the scatter distribution through the analysis of the images themselves and the estimation of the tested object properties, and adopt the post-processing methods to correct the scatter. The software methods mainly include convolution,[12,13] deconvolution,[14] the Monte Carlo (MC) simulation method,[15–17] and so on. The MC method, which uses the computer simulation to obtain the image scatter distribution, is an effective and accurate scatter correction method, but is mostly limited to theoretical studies because of its time-consuming calculation.

As a result of using plane array detectors in the CBCT, the scatter field shows a two-dimensional distribution. Then satisfactory results cannot be obtained through a single hardware or software method. So, there have been some hybrid correction methods combining hardwares and softwares, for example, the beam-stop array,[18] beam-hole array,[19] beam attenuation array,[20] stationary beam blocker,[21,22] moving blocker strips,[23,24] attenuation plate imaging,[25] and the pri-

*Project supported by the National Science and Technology Major Project of the Ministry of Industry and Information Technology of China (Grant No. 2012ZX04007021), the Young Scientists Fund of the National Natural Science Foundation of China (Grant No. 51105315), the Natural Science Basic Research Program of Shaanxi Province, China (Grant No. 2013JM7003), and the Northwestern Polytechnical University Foundation for Fundamental Research, China (Grant Nos. 3102014KYJD022 and JC20120226).

†Corresponding author. E-mail: kdhuang@nwpu.edu.cn

© 2014 Chinese Physical Society and IOP Publishing Ltd

mary ray modulation correction method.[26,27] In addition, someone has simulated the scatter from the perspective of secondary radiation.[28] These methods, which are usually under some approximation assumptions, have achieved good scatter correction results in the medical CT imaging. However, the applicability of the methods used in the middle- and the high-energy X-ray scans of the industrial CT imaging needs to be researched and tested further.

A new method of CBCT scatter suppression and correction based on the interlacing-slit scan is proposed in this article. This method can complete the scatter suppression outside the FPD and the scatter estimation within the FPD at the same time, so the scatter correction result, which is more in line with the actual scatter condition in CBCT imaging systems, can be obtained. The feasibility and practicality of this method are verified through the experiments.

2. Scheme design of scatter suppression scan

2.1. Design of the scatter suppression plate with interlacing slits

The basic idea of scatter suppression based on the interlacing-slit scan is to make use of the good inhibition of the slits on the scatter ray, image the two slit regions respectively (the slits of the two regions are interlaced), and then splice out a complete set of scatter suppression projection images. According to the characteristics of the CBCT imaging system based on an FPD, we analyze and design the scatter suppression plate with interlacing slits from the following aspects.

(i) The suppression plate must be sufficient to fully shield the X-ray transmission in the range of voltage used. On this basis, the thicker the suppression plate is, the better the scatter suppression result can be.

(ii) The suppression plate is divided into two imaging regions which have some parallel slits, and the slits of the two areas remain interlacing.

(iii) Theoretically, the narrower the slits are, the better the scatter suppression result can be. However in order to make full use of the initial ray intensity of the ray source, the width of the slits cannot be smaller than the size of the ray source focus.

(iv) To obtain a complete image of the tested object and to satisfy the need of the splice computing of the projection images, the width of the blocker strips between the slits should be smaller than the width of the slits.

(v) Taking the imaging cone angle of the CBCT scan into account, the slit angles need to concentrate on the ray source focus, which can make the penumbral regions of the slits smallest under the condition of cone beam imaging.

(vi) To ensure no reduction of the detector's effective imaging area, the slit coverage of the left or right imaging area in the plate needs to be larger than the detector's imaging window.

The X-ray source of the experimental CBCT system is Y.TU 450-D02 of YXLON, whose focus is 2.5/5.5 mm and maximum voltage is 450 kV. The FPD is PaxScan 2520 of Varian. Based on the above analysis, taking the ray shielding, economy, and workability of the scatter suppression plate with interlacing slits into account, we designed the plate shown in Fig. 1, with slit width $W = 8$ mm, slit spacing $S = 15$ mm, plate thickness $T_1 = 40$ mm; the material used is lead-antimony alloy (5% antimony).

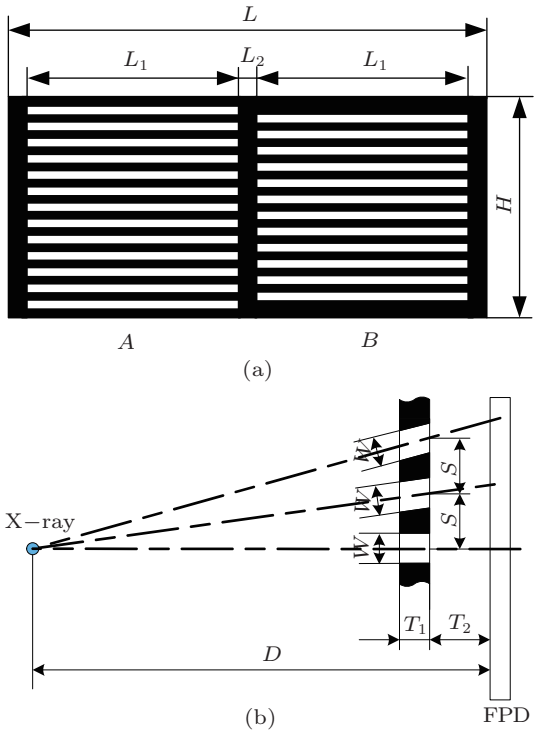


Fig. 1. (color online) Design diagram of the scatter suppression plate with interlacing slits: (a) front structures, (b) structural diagram of the slits in the imaging region *A*.

There are two placement options of the scatter suppression plate with interlacing slits. One is to put it between the tested object and the FPD (position 1), the other is to put it between the tested object and the ray source (position 2). For position 1, the X-rays pass through the tested object first and then pass through the plate. In this case, only a small number of scatter photons can pass through the slits to the FPD. For position 2, the X-rays are collimated by the slits and then interact with the tested object, and both scatter photons and penetration photons can reach the FPD. We choose position 1 to place the plate and make it as close as possible to the FPD.

The scatter suppression plate needs to be moved in the process of the CBCT scan. In order to achieve the automation and continuity of the scan, we fix the plate on a translational worktable, whose movement control is integrated with the CBCT scan system. In addition, in order to suppress the

scatter from peripheral objects, the beam-limited block is fixed on the exit of the ray source, and the non-image area of the FPD is shielded. The design schematic diagram and the actual system picture of the scatter suppression plate imaging are shown in Fig. 2.

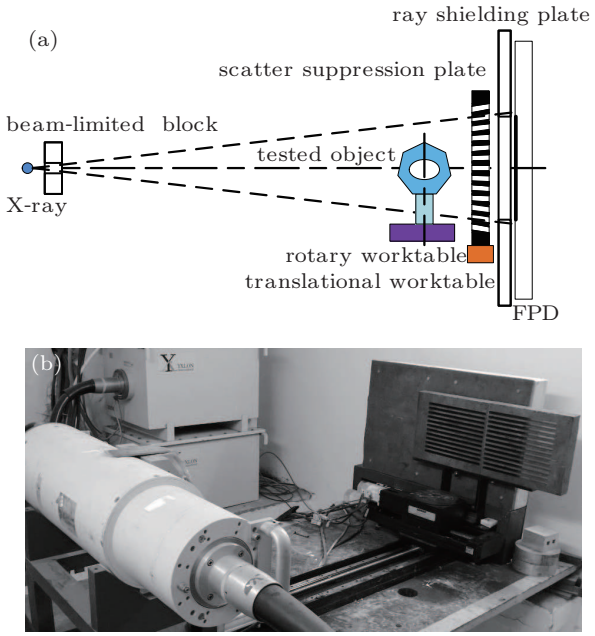


Fig. 2. (color online) Installation diagram of the scatter suppression plate with interlacing slits: (a) schematic diagram, (b) actual system picture.

2.2. Steps of the scatter suppression scan with interlacing slits

The CBCT scatter suppression based on the interlacing-slit scan needs four groups of projection images, and the specific steps are as follows.

(i) Determine the scan parameters of the CBCT system, and keep them unchanged during the entire scan.

(ii) Collect some projection images of slit *A*, and obtain one projection image after averaging them, which is called image 1.

(iii) Place the tested object on the rotary worktable, and then collect a group of projection images of slit *A* plus the object through a circle scan, which are called image 2.

(iv) Keep the tested object still (the starting position is the same as that in step 3), move the scatter suppression plate, and then collect a group of projection images of slit *B* plus the object through a circle scan, which are called image 3.

(v) Remove the tested object, collect some projection images of slit *B*, and obtain one projection image after averaging them, which is called image 4.

Image 1 and image 4 are used to obtain the fusion coefficient image, generally only a little time is needed to collect the images. If the same or similar scan parameters are used, the fusion coefficient image obtained before can be reused in the scatter correction, in this case, step (ii) and step (v) can be omitted.

3. Imaging analysis and scatter correction calculation

The CBCT scan experiment with the scatter suppression plate is carried out for an aluminum part. The scan voltage is 180 kV, the exposure is 0.2178 mA·s, the number of collected projection images of step (ii) and step (v) is both 9, and those of step (iii) and step (iv) are both 360. The image resolution is 1024×1024. One of each group of the projection images scanned with the interlacing slits is shown in Fig. 3, and the grayscale comparison of the interlacing-slit scan is shown in Fig. 4.

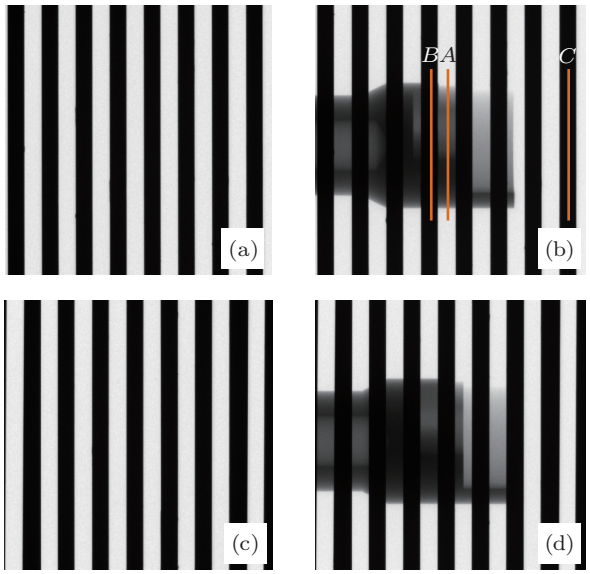


Fig. 3. (color online) Projection images of interlacing-slit scan (grayscale window: [98, 2827]): (a) projection image of slit *A*, (b) projection image of slit *A* and the part, (c) projection image of slit *B*, (d) projection image of slit *B* and the part.

It can be seen from Fig. 4(a) that compared with slit imaging and open imaging, the grayscale in the slit region decreases 150–230 approximately. Since all scan parameters are consistent, this part of decreasing grayscale can be considered as the suppression of the scatter photons by the slits.

From Fig. 4(b), it can be seen that there are apparent outputs in the blocker strip regions of the scatter suppression plate. However, according to the design parameters of the plate, the regions are not likely to be irradiated by penetration rays. So the outputs must be the contribution of the scatter. As the range of the visible light scatter of the scintillator is small and the width of the blocker strip is bigger, the main source of the outputs must be the ray scatter, which is caused by the related structures within the FPD. It is called the inner scatter of the FPD in this article.

It can be seen from Fig. 4(b) that there are obvious differences between the blocker strip region's covered and not covered parts. The grayscale of the blocker strip region's covered part is significantly lower, and the thicker the part is, the

lower the grayscale will be. This means that the scatter distribution within the FPD is not uniform. It is related with the distribution of the received radiation in adjacent slit regions.

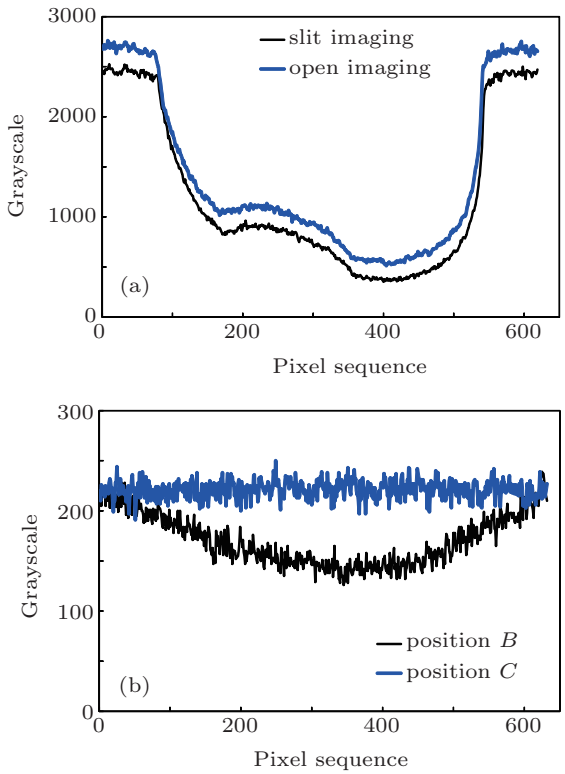


Fig. 4. (color online) Grayscale comparison on the lines in Fig. 3(b): (a) slit imaging and open imaging on position *A*, (b) position *B* and position *C*.

Due to the existence of the inner scatter of the FPD, the grayscale of the slit regions must include the contribution of the inner scatter. According to the experimental analysis, the distribution of the inner scatter is relatively smooth, so it is possible to make use of the inner scatter of the blocker strip regions in slits *A* and *B* to acquire the integral scatter within the FPD in some manner. It is noteworthy that the projection images of both slits *A* and *B* (regardless of including or excluding the part) contain an inner scatter field. So it needs to be removed in the calculation of the scatter correction.

Based on the four groups of images obtained through the scatter suppression scan with interlacing slits for CBCT and the above-described imaging analysis, we propose a scatter correction calculation method for the CBCT based on image fusion, and the specific steps are as follows.

(i) According to image 1 and image 4, calculate the inner scatter field S_w without the tested object as follows.

1) Search for the maximum grayscale pixel in image 1 and calculate its neighborhood average, which is denoted as q.

2) Determine the segmentation threshold of the blocker strip regions, $g = q/\eta$, where η is general 7–9.

3) Generate two template images F_1 and F_2 which are the same size as image 1, and set the initial values of them to 0.

4) Traversal image 1, and if the neighborhood grayscale average of the pixel is less than g, set the corresponding pixel in F_1 to 1.

5) Traversal image 4, and if the neighborhood grayscale average of the pixel is less than g, set the corresponding pixel in F_2 to 1.

6) Obtain S_1 by multiplying image 1 and F_1 correspondingly, and obtain S_2 by multiplying image 4 and F_2 correspondingly.

7) Obtain S'_w by adding S_1 and S_2 correspondingly.

8) Make a copy of S'_w, called S_w, calculate the neighborhood summation t of the pixel whose grayscale is 0 in S'_w, and the number of non-zero pixels in the neighborhood is n, then the grayscale of the pixel is $s = t/n$, store s to the corresponding location in S_w.

(ii) Calculate fusion coefficient image R according to image 1 and image 4 as follows.

1) Plus image 1 and image 4 correspondingly and then minus $2S_w$ to obtain image J.

2) Set up $\overline{J}$ as the average value of J, then $R_{x,y} = \overline{J}/J_{x,y}$.

(iii) According to every corresponding angle projection image of image 2 and image 3, which are called I_1 and I_2, calculate the inner scatter field S_y with the tested object as follows.

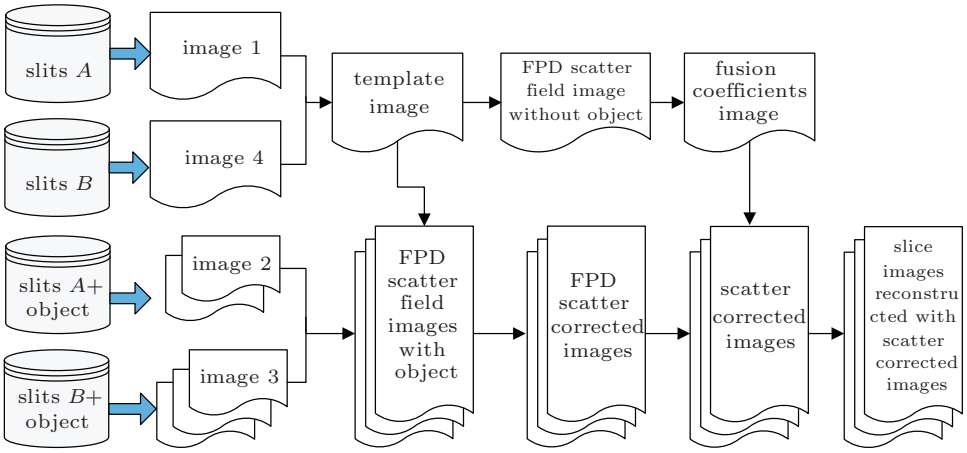


Fig. 5. Overall flowchart of the scatter correction based on an interlacing-slit scan.

1) Obtain S_1 by multiplying I_1 and F_1 correspondingly, and obtain S_2 by multiplying I_2 and F_2 correspondingly.

2) Obtain S'_y by adding S_1 and S_2 correspondingly.

3) Make a copy of S'_y, called S_y, calculate the neighborhood summation t of the pixel whose grayscale is 0 in S'_y, and the number of non-zero pixels in the neighborhood is n, then the grayscale of the pixel is $s = t/n$, store s to the corresponding location in S_y.

(iv) Plus I_1 and I_2 correspondingly and then minus $2S_y$ to obtain image C'.

(v) Obtain the final scatter suppression and correction image by multiplying C' and R correspondingly.

By the CBCT reconstruction with a set of scatter suppression and correction projection images (FDK reconstruction algorithm commonly), the scatter corrected slice images of the tested object can be obtained. The overall flowchart of the scatter correction based on the interlacing-slit scan is shown in Fig. 5.

4. Experiment and analysis

Figure 6 is the images from the scatter suppression and correction experiment for the CBCT based on the interlacing-slit scan. It can be seen that the grayscale of the scatter corrected image decreases significantly, and the absolute value decreased in the blank area is a little larger than that in the area with the tested object.

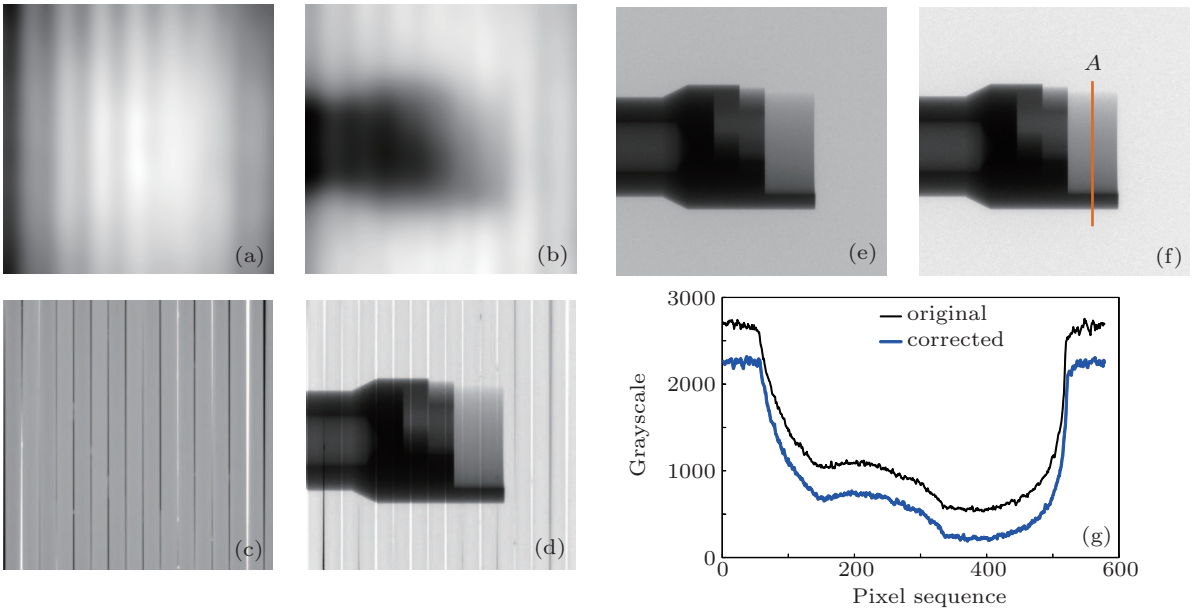


Fig. 6. (color online) Experimental results of CBCT scatter suppression and correction based on interlacing-slit scan: (a) FPD scatter field image without object, (b) FPD scatter field image with object, (c) fusion coefficient image, (d) FPD scatter corrected image, (e) scatter corrected image, (f) original projection image, and (g) grayscale comparison on the same line A. Grayscale window: (a) [264, 325], (b) [128, 251], (c) [0.52, 1.3], (d) , (e), and (f) [98, 2827].

Figures 7 and 8 show the comparison of the 500$^{\text{th}}$ and the 572$^{\text{th}}$ slice images before and after the scatter correction, where rectangle A is the comparison position of the signal to noise ratio (SNR),[29] rectangle B is the comparison position of the contrast to noise ratio (CNR)[29] and average gradient (AG),[30] and line C is the comparison position of grayscale. It can be seen from the pictures that the contour sharpness of the scatter corrected slice images is improved significantly, and this improvement is more outstanding in the parts of inner concave contours. On the other hand, we observe that the noise in the scatter corrected slice images has a certain degree of magnification, this is because the interlacing-slit scan method decreases the amount of X-ray photons received by the FPD and the noise of the penetration rays is relatively stable, the proportion of the noise in the projection images is increased after the scatter correction, and the noise in the scatter corrected slice images is amplified correspondingly.

Table 1 is the numerical comparison of slice image quality of the 500$^{\text{th}}$ and the 572$^{\text{th}}$ slice images before and after the scatter correction in Figs. 7 and 8. It can be clearly seen from the table that the SNR of the slice images processed by the scatter correction decreases significantly, and that of the 500$^{\text{th}}$ slice image, which comes from a thicker part, decreases more than that of the 572$^{\text{th}}$ slice image, which comes from a thinner part. This is consistent with the previous analysis. While the other two evaluation items, CNR and AG, both increase obviously, especially in the parts of inner concave contours, AG has a great raise. This means that the scatter correction is directly effective to improve the sharpness of the internal contour structures.

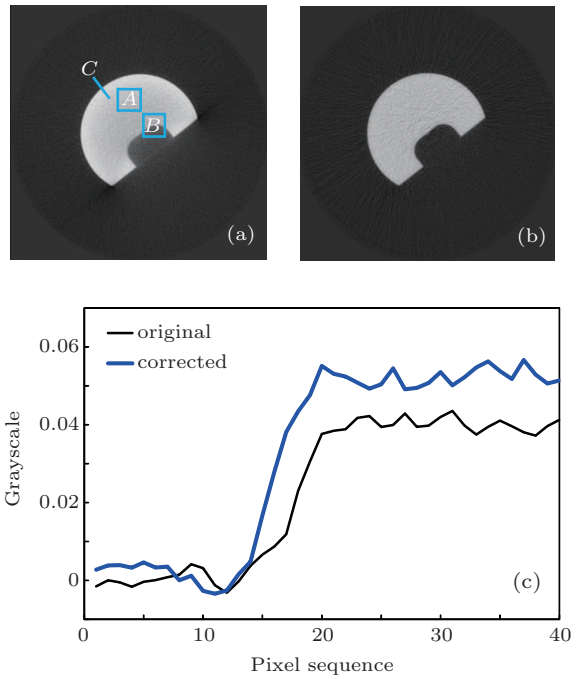


Fig. 7. (color online) Comparison of the 500th slice image before and after scatter correction (grayscale window: [–0.012, 0.068]): (a) original slice image, (b) scatter corrected slice image, (c) grayscale comparison on the same location.

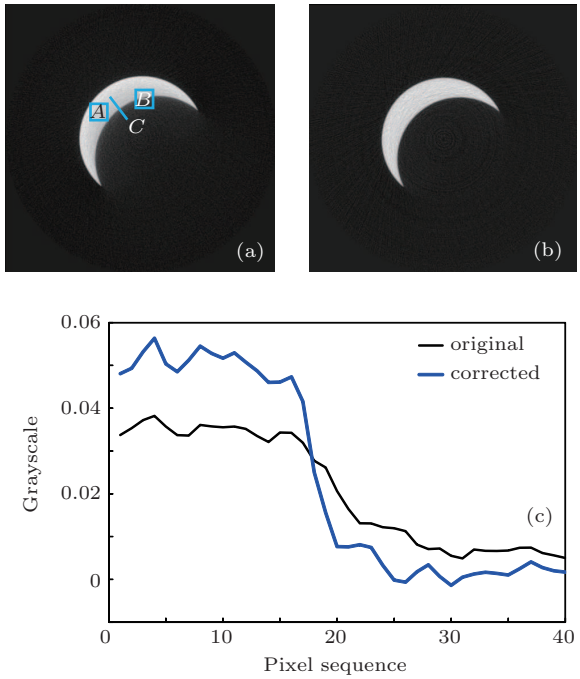


Fig. 8. (color online) Comparison of the 572th slice image before and after scatter correction (grayscale window: [–0.012, 0.068]): (a) original slice image, (b) scatter corrected slice image, (c) grayscale comparison on the same location.

Table 1. Numerical comparison of slice image quality before and after the scatter correction.

Slice number		SNR		CNR		AG	
		value	increased/%	value	increased/%	value	increased/%
500th	original	13.08	/	6.095	/	0.001560	/
	corrected	9.597	–26.63	6.810	11.73	0.003546	127.31
572th	original	21.89	/	6.337	/	0.001157	/
	corrected	18.66	–14.76	7.479	18.02	0.002168	87.38

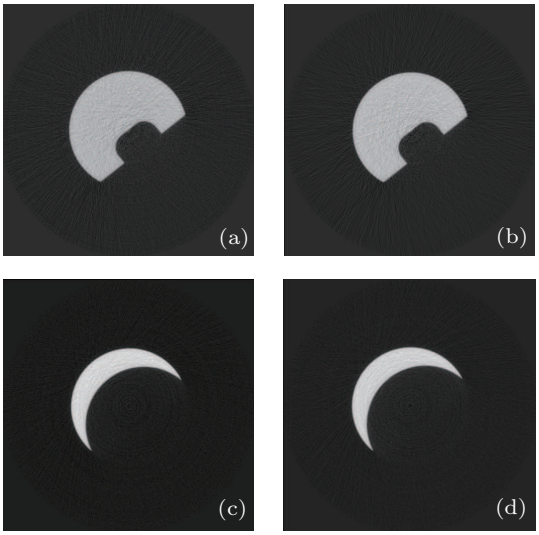


Fig. 9. (color online) Scatter correction comparison of slice images with different exposure levels (grayscale window: [–0.012, 0.068]): (a) the 500th slice with 0.2178 mA·s, (b) the 500th slice with 0.2343 mA·s, (c) the 572th slice with 0.2178 mA·s, (d) the 572th slice with 0.2343 mA·s.

In order to test the cause analyzed above for the SNR reduction in the scatter corrected slice image, we increase the scan exposure from 0.2178 mA·s to 0.2343 mA·s, keeping the experiment environment and the correction method unchanged. This can make the grayscale of the blank area in slit imaging consistent with that in open imaging. The purpose is to make the ray strength received by the FPD the same before and after the scatter suppression. Figure 9 is the scatter correction comparison of the 500th and the 572th slice images before and after the increasing exposure. No apparent difference can be seen from the images, but we know that increasing the exposure can reduce the noise. The numerical comparison of slice image quality is shown in Table 2 (the evaluation regions are the same as those in Figs. 7 and 8). It can be seen from the table that SNR and CNR are both improved, and SNR is more obviously improved. AG cannot completely distinguish structures and noises, so there is a slight lowering of AG. By a further analysis, we can see that although increasing exposure can compensate for the loss of the ray strength caused by the scatter suppression, the method not only suppresses the outer scatter but also corrects the inner scatter of the FPD, and decreases the image grayscale in the form. The exposure should be further increased if we want to achieve the SNR level as open imaging.

Table 2. Numerical comparison of slice image quality with different exposure levels.

Slice number		SNR		CNR		AG	
		value	increased/%	value	increased/%	value	increased/%
500^{th}	0.2178 mA·s	9.597	/	6.810	/	0.003546	/
	0.2343 mA·s	10.19	6.18	6.915	1.54	0.003517	–0.82
572^{th}	0.2178 mA·s	18.66	/	7.479	/	0.002168	/
	0.2343 mA·s	19.87	6.48	7.675	2.62	0.002138	–1.38

5. Conclusion

Based on the analysis of the existing methods, a scatter correction method for CBCT based on the interlacing-slit scan is proposed in this article. Firstly, according to the characteristics of CBCT imaging, a scatter suppression plate with interlacing slits is designed and fabricated. Then a scatter correction calculation method for CBCT based on image fusion is proposed, which can splice out a complete set of scatter suppression projection images and simultaneously complete the scatter correction within the FPD. Finally, the overall process of scatter suppression and correction is provided. The experimental results show that this method can significantly improve the clarity of the slice images and achieve a good scatter correction. If the interlacing slits are dense enough, the scatter suppression result of CBCT can be close to that of the fan-beam CT in theory. The method is also suitable for small-focus and micro-focus CT systems.

This method may cause SNR loss to a certain extent, which can be compensated by increasing the exposure. In addition, due to the projection cone angle of the slits in the scatter suppression plate, this method can only be used when the distance between the ray source and the detector is constant or has only small changes. For the problem that two circle scans of interlacing slits may lower the detection efficiency, we may increase the scan speed and the exposure, which can further improve this method.

References

[1] Luo Z Y, Yang X Q, Meng Y Z and Deng Y 2010 *Acta Phys. Sin.* **59** 8237 (in Chinese)

[2] Wang X C, Yan B, Liu H K, Li L, Wei X and Hu G E 2013 *Acta Phys. Sin.* **62** 098702 (in Chinese)

[3] Guo X L, Tang Z W, Zhang H and Hu G S 2010 *J. Tsinghua Univ. (Sci. & Tech.)* **50** 450

[4] Ding G X, Duggan D M and Coffey C W 2007 *Phys. Med. Biol.* **52** 1595

[5] Morin O, Gillis A, Chen J, Aubin M, Bucci M K, Roach M 3rd and Pouliot J 2006 *Med. Dosim.* **31** 51

[6] Kwan A L, Boone J M and Shah N 2005 *Med. Phys.* **32** 2967

[7] Siewerdsen J H and Jaffrey D A 2001 *Med. Phys.* **28** 220

[8] Boone J M 1986 *Med. Phys.* **13** 319

[9] Neitzel U 1992 *Med. Phys.* **19** 475

[10] Graham S A, Moseley D J, Siewerdsen J H and Jaffray D A 2007 *Med. Phys.* **34** 2691

[11] Coates A M, Dixon A M and Huckle J 2012 *Radiography* **18** 250

[12] Li Q L, Yan B, Li L, Sun H S and Zhang F 2012 *High Power Laser and Particle Beams* **24** 2235

[13] Naimuddin S, Hasegawa B H and Mistretta C A 1987 *Med. Phys.* **14** 330

[14] Deng Z S, Ni D P, Jiang D Z, Zhao Z H, Xiao F and Xu L J 1997 *J. Biomed. Eng.* **14** 137 (in Chinese)

[15] Jia P X, Zhang F, Yan B and Bao S L 2010 *Chin. Phys. B* **19** 087802

[16] Mettivier G, Lanconelli N, Meo S L and Russo P 2012 *IEEE Trans. Nucl. Sci.* **59** 2008

[17] Baer M and Kachelrie M 2012 *Phys. Med. Biol.* **57** 6849

[18] Ning R, Tang X Y and Conover D 2004 *Med. Phys.* **31** 1195

[19] Schörner K, Goldammer M and Stephan J 2011 *Nucl. Instr. Meth. Phys. Res. B* **269** 292

[20] Zhang D H, Hu D C, Huang K D and Kong Y M 2009 *Chin. Mech. Eng.* **20** 639 (in Chinese)

[21] Niu T Y and Zhu L 2011 *Med. Phys.* **38** 6027

[22] Dong X, Jia X, Niu T Y and Zhu L 2012 *Proc. SPIE Medical Imaging 2012: Physics of Medical Imaging*, February 4–9, 2012 San Diego, USA, p. 831319

[23] Wang J, Mao W and Solberg T 2010 *Med. Phys.* **37** 5792

[24] Ouyang L, Song K and Wang J 2013 *Med. Phys.* **40** 071903

[25] Xie S P and Luo L M 2011 *Acta Electron. Sin.* **39** 1708 (in Chinese)

[26] Zhu L, Bennett N R and Fahrig R 2006 *IEEE Trans. Med. Imaging* **25** 1573

[27] Gao H W, Fahrig R, Bennett N R, Sun M S, Star-Lack J and Zhu L 2010 *Med. Phys.* **37** 934

[28] Wils P, Létang J M and Bruandet J P 2012 *J. Electron. Imaging* **21** 021113

[29] Zhang H, Huang K D, Shi Y K and Li M J 2012 *CT Theory and Applications* **21** 247 (in Chinese)

[30] Huang K D, Zhang D H, Li M J and Zhang H 2013 *Acta Phys. Sin.* **62** 210702 (in Chinese)